Lawrence Berkeley National Laboratory

Title
Impact of deposition conditions on the crystallization kinetics of amorphous GeTe films

Authors
Khoo, Chee Ying
Liu, Hai
Sasangka, Wardhana A
et al.

CrossMark

Impact of deposition conditions on the crystallization kinetics of amorphous GeTe films

Chee Ying Khoo[1,2] · Hai Liu[1] · Wardhana A. Sasangka[3] · Riko I. Made[3] ·
Nobu Tamura[4] · Martin Kunz[4] · Arief S. Budiman[5] · Chee Lip Gan[1,2,3] ·
Carl V. Thompson[2,3,6]

Abstract The speed at which phase change memory devices can operate depends strongly on the crystallization kinetics of the amorphous phase. To better understand factors that affect the crystallization rate, we have investigated crystallization of GeTe films as a function of their deposition temperatures and deposition rates, using X-ray synchrotron radiation and Raman spectroscopy. As-deposited films were found to be fully amorphous under all conditions, even though films deposited at higher temperatures and lower rates experienced lower effective quench rates. Non-isothermal transformation curves show that the apparent crystallization temperature of GeTe films decreases with increasing deposition temperature and decreasing deposition rate. It was found that this correlates with a decrease in the activation energy for nucleation (calculated using Kissinger's analysis), while the activation energy for crystal growth remained unaffected. From Raman spectroscopy measurements, it was found that increasing the deposition temperature or decreasing the deposition rate, and therefore the effective quench rate, reduces the number of homopolar Te–Te bonds and thereby reduces the barrier to crystal nucleation.

✉ Carl V. Thompson
cthomp@mit.edu

Chee Lip Gan
clgan@ntu.edu.sg

1 School of Materials, Science and Engineering, Nanyang Technological University, Singapore 639798, Singapore

2 Advance Materials for Micro- and Nano-Systems, Singapore-MIT Alliance, Singapore 117576, Singapore

3 Low Energy Electronic Systems, Singapore-MIT Alliance for Research and Technology, Singapore 138602, Singapore

4 Advance Light Source, Lawrence Berkeley National Lab, Berkeley, CA 94720, USA

5 Engineering Products Development (EPD) Pillars, Singapore University of Technology and Design, Singapore 138682, Singapore

6 Department of Materials Science and Engineering, Massachusetts Institute of Technology, Cambridge, MA 02139, USA

Introduction

In the mid-1960s, Ovshinsky proposed the idea of phase change recording [1]. Phase change materials (e.g., $Ge_2Sb_2Te_5$ and GeTe) undergo a reversible transformation between crystalline and amorphous states when subjected to laser-induced or current-induced heating and quenching [2, 3]. The attractiveness of phase change materials lies in their very large changes in electrical resistivity and optical reflectivity when switching between these two states [4–6]. This phenomenon is currently used in optical information storage and is under wide-spread investigation for use in electrical information storage devices [7, 8]. The operation of these devices strongly depends on the crystallization temperatures and crystallization rates of the materials, and therefore, a detailed understanding of factors that influence the kinetics of crystallization is critical. Studies of amorphous $Ge_2Sb_2Te_5$ and GeTe films prepared using different methods, such as sputtering, melt-quenching, and ion-irradiation, have been carried out [9, 10]. The local order of these amorphous films has been examined using Raman spectroscopy and was found to be significantly different [9,

10]. These differences were found to correlate with differences in crystallization temperatures [9, 10].

In this work, we report studies of the crystallization kinetics of amorphous GeTe thin films as a function of deposition temperature and deposition rate. The crystallization temperature was determined using X-ray synchrotron radiation during in-situ annealing. Effective activation energies for the crystallization process were determined using Kissinger's analysis [11]. The local order of the as-deposited amorphous GeTe films was analyzed using micro-Raman spectroscopy.

Experimental procedures

1-μm-thick GeTe films were deposited by RF-magnetron sputtering from stoichiometric targets onto Si substrates coated with thin layers of native SiO_2. The background pressure before sputtering was maintained at $\sim 10^{-6}$ Torr. With the presence of argon gas during sputtering, the pressure was maintained at 10^{-3} Torr. A first set of samples was deposited on substrates at room temperature, 60, 80, and 100 °C, with a deposition rate of 8 nm/min. For a second set of samples, films were deposited at room temperature using different rates, 7.1 nm/min, 8.8 nm/min, and 10.3 nm/min, by varying the argon gas pressure. For both sets of experiments, real-time synchrotron X-ray diffraction with a 2D detector and monochromatic beam (energy = 10 keV, $\lambda = 0.124$ nm) at beamline 12.3.2 of the advanced light source in the Lawrence Berkeley National Laboratory was used to monitor the crystallization. Each exposure time was set to be 60 s. The synchrotron X-ray beam has a final focus size of 2 μm (v) $\times$ 8 μm (h) (FWHM). The diffraction patterns were collected with a DECTRIS Pilatus 1 M pixel area detector (active area of 179 mm $\times$ 169 mm), which was placed at a distance of approximately 140 mm from the sample. More detailed information on the setup at this beamline can be obtained elsewhere [12, 13].

All samples were annealed at a constant rate of 2, 5, or 10 °C/min from room temperature to 230 °C, a temperature at which they were fully crystalline. Transformation curves at different heating rates were obtained by determining the fraction of the film that had transformed as a function of temperature. The microstructures of the GeTe films were characterized using energy dispersive X-ray spectroscopy (EDX) and transmission electron microscopy (TEM). A focused ion beam (FIB) system with dual-beam capability was used to prepare the TEM samples, and a JEOL TEM 2100F with an accelerating voltage of 200 kV was used to examine the as-deposited films. EDX was used to determine the composition of the films.

All the as-deposited amorphous GeTe thin films were also analyzed by means of micro-Raman spectroscopy. The samples were excited with a He–Ne laser ($\lambda = 633$ nm), and the incident laser power was adjusted to 0.5 mW in order to minimize heating effects in the illuminated sample region of interest [9, 14]. The Raman spectra were recorded at an interval of 0.4 cm^{-1}. Accumulation times of 3 min were sufficient to obtain a satisfactory signal-to-noise ratio.

Results and discussion

Effect of deposition temperatures

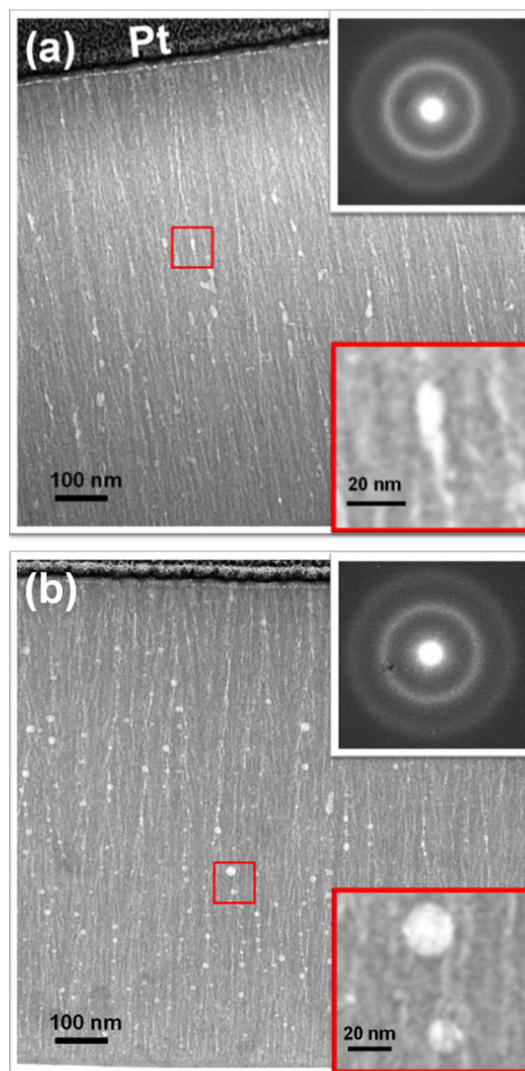Figure 1 shows bright-field TEM images of GeTe films deposited at room temperature and 100 °C. Cross-sectional

Fig. 1 Bright-field TEM images of cross sections of GeTe films deposited at **a** room temperature and **b** 100 °C on Si substrates coated with thin layers of native oxide. *Top right insets* show electron diffraction patterns and *bottom right insets* show high magnification views of nano-scale voids within the film. Pt layers on *top* of the films act as protective layers during FIB sample preparation

TEM images reveal that all as-deposited films were fully amorphous, but with columnar structures and nano-scale voids. The latter is not uncommon in amorphous films deposited using sputter deposition [15, 16]. The inset electron diffraction patterns confirm that the films were amorphous as deposited, which was also supported by X-ray diffraction (XRD) analysis. From EDX, the composition of the films was determined to be $Ge_{43}Te_{57}$ ($\pm$ 1% error), which is Te-rich.

Debye-Scherrer rings were generated based on diffraction intensities from the 2D detector integrated in the azimuthal direction. Figure 2 shows XRD results obtained by transforming 2D synchrotron data using XMAS, a software developed in-house at beamline 12.3.2 [17]. The as-deposited films were amorphous at all deposition temperatures, as shown in Fig. 2a. After annealing to 230 °C, the films were found to be fully crystallized, as shown in Fig. 2b. Regardless of the deposition temperatures, the GeTe films were composed of the same phase, with the

expected trigonal symmetry [18]. Weak Te peaks were also observed due to the Te-rich composition of the films.

Figure 3a shows transformation curves for crystallization of GeTe, based on the maximum intensity of the (011) peak normalized by the maximum intensity of this peak after full transformation at 230 °C. The sample was heated at a rate of 2 °C/min from room temperature to 230 °C. The apparent crystallization temperature was defined as the temperature at which half of the sample was crystallized [19]. The apparent crystallization temperatures observed in this study are higher than values reported by others, as determined from optical reflectivity measurements [20, 21]. This is expected as all the films here are Te-rich in composition. From the transformation curves, it is clearly seen that the apparent crystallization temperatures decrease with increasing deposition temperature. Figure 3b shows transformation curves for GeTe films deposited at room
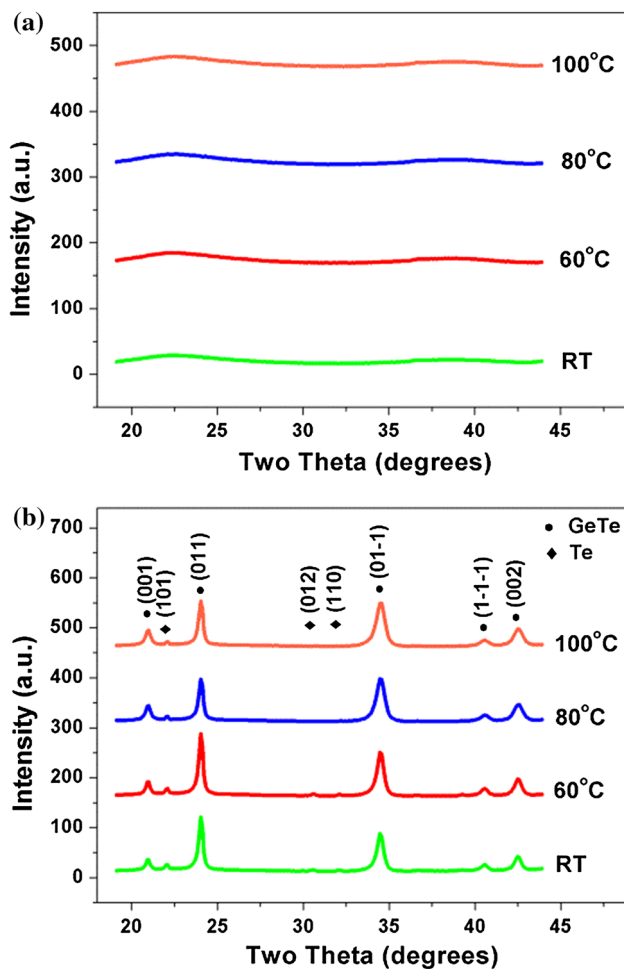

Fig. 2 XRD results for GeTe films. **a** As-deposited and **b** fully crystallized at 230 °C, for films deposited at different substrate temperatures (room temperature, 60, 80, and 100 °C)
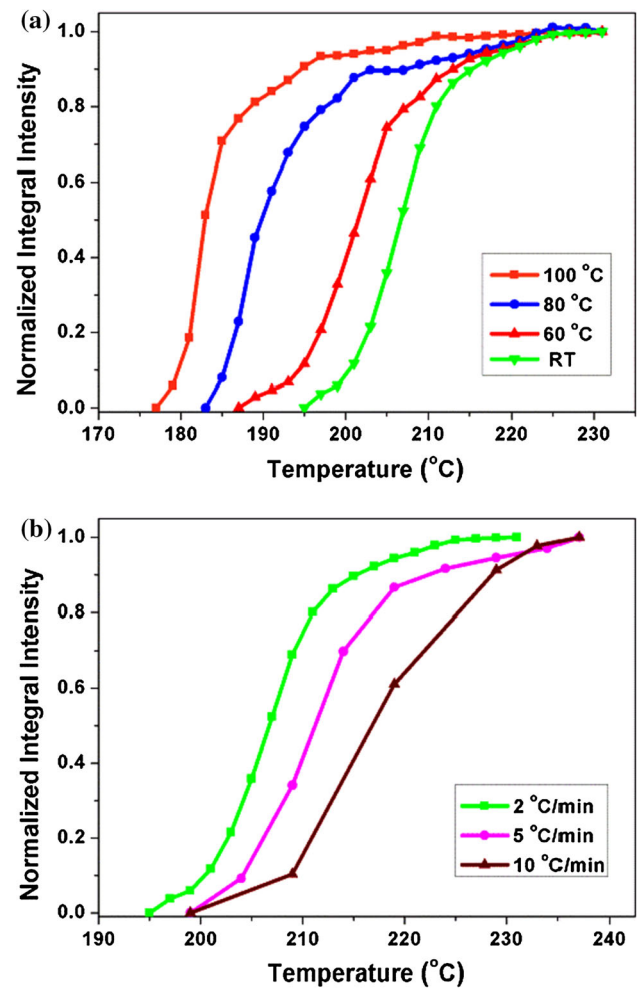

Fig. 3 **a** Transformation curves for GeTe films deposited at different temperatures, based on normalized magnitudes of the (011) peak observed at 230 °C. The heating rate was 2 °C/min. **b** Transformation curves for GeTe films deposited at room temperature and heated at different rates

temperature and heated at different rates: 2, 5, and 10 °C/min. As expected, the apparent crystallization temperature increases with increasing heating rate [22, 23].

Figure 4a shows the local effective activation energy E_c as a function of the fraction transformed α. E_c was determined using the Kissinger method for various values of α for data obtained at different heating rates shown in Fig. 3b [11]. The Kissinger equation can be written as follows:

$$\ln\left(\frac{\beta}{T_c^2}\right) = -\frac{E_c}{kT_c} + \text{const}, \tag{1}$$

where β is the heating rate, k is Boltzmann's constant, E_c is the activation energy at a particular transformed fraction α, and T_c is the temperature at which the transformed fraction α is reached.

The dependence of E_c on the fraction transformed is affected by changes in the nucleation and growth behavior

(a)

(b)

Fig. 4 **a** The local effective activation energy E_c as a function of the fraction transformed α for films prepared at various deposition temperatures and **b** activation energies for nucleation and growth as a function of the deposition temperature

during the crystallization process [24–26]. The local activation energy $E_c(\alpha)$ is composed of two parts: the activation energy of nucleation (E_n) and the activation energy of growth (E_g) [27–29]. E_c at a given α can be written as

$$E_c = aE_n + bE_g (I \geq 0, \ U \geq 0), \tag{2}$$

where I and U are the steady-state nucleation rate and growth velocity, respectively, with a and b being variables related to the Avrami parameter, having values $0 \leq a$, $b \leq 1$ and $a + b = 1$ [28, 29]. In the early stage of transformation, with lower values of α, crystallization is dominated by nucleation, whereas at later stages, with higher values of α, crystallization is dominated by growth. Fitting the plot in Fig. 4a using a non-linear regression method (shown using dotted lines), we estimated the value of the activation energies for nucleation and growth, E_c ($\alpha = 0$) = E_n and growth $E_c(\alpha = 1) = E_g$, respectively. The fitting was carried out under the assumption that the values of a and b at a particular value of α are the same for all deposition temperatures. Figure 4b shows values of the activation energies for nucleation and growth obtained from Fig. 4a. It is seen that the activation energy for nucleation decreases significantly with increasing deposition temperature, from 4.0 to 2.6 eV. In contrast, the activation energy for growth remains relatively constant at 2.0 eV. Thus, the decrease in the effective activation energy for crystallization of GeTe observed for increasing deposition temperatures is primarily due to a reduction in the activation energy for nucleation. Similar activation energies for nucleation and growth of films deposited at room temperature have been reported elsewhere using a different technique [10, 30]. Films deposited at room temperature experience a higher effective quench rate as compared to films deposited at higher temperatures [31]. We postulate that this results in fewer clusters that can act as precursors of crystalline nuclei, thus making nucleation more difficult. That the activation energy for growth is unaffected by the deposition conditions may explain why it has been found in other studies that samples having the same composition but made under different conditions have the same temperature dependence for crystallization, while differences in the crystallization rate are still observed due to differences in the nucleation rates [32, 33].

Figure 5 shows Raman spectra for GeTe films deposited at different temperatures. For all the Raman spectra, there are peaks found at 88, 120, 139, and 160 cm^{-1}. The broad peaks found at 88 and 160 cm^{-1} are contributed by GeTe vibration modes [14, 34, 35]. Two distinct peaks were also observed at 120 and 139 cm^{-1}, and their intensities decreased with increasing deposition temperature. It is known that crystalline Tellurium has strongest peaks at 120.4 $\pm$ 0.5 and 140.7 $\pm$ 0.5 cm^{-1} [36]. The close proximity of the observed peaks suggests the presence of
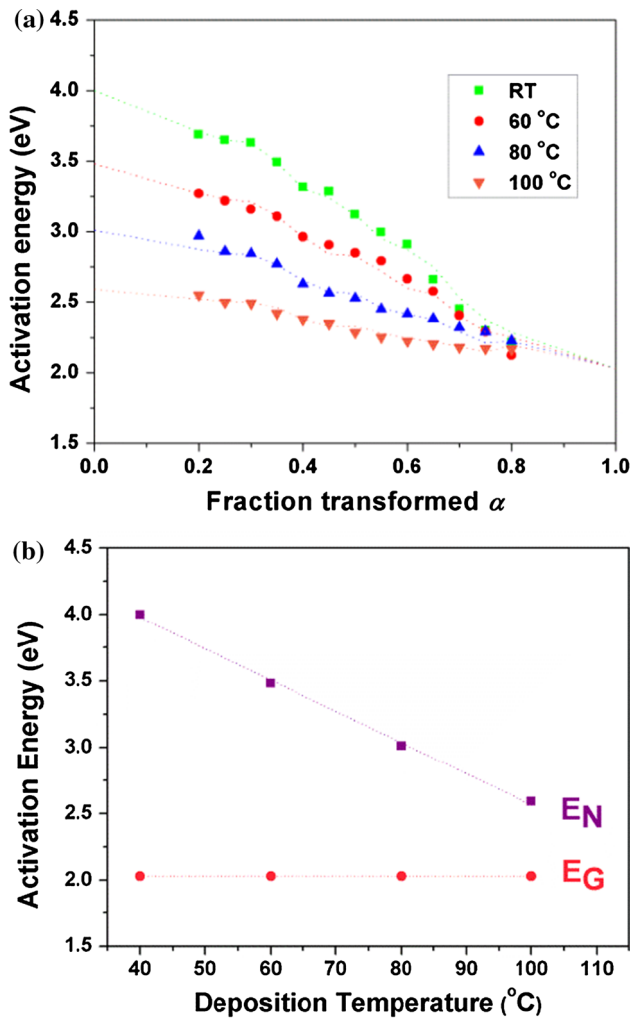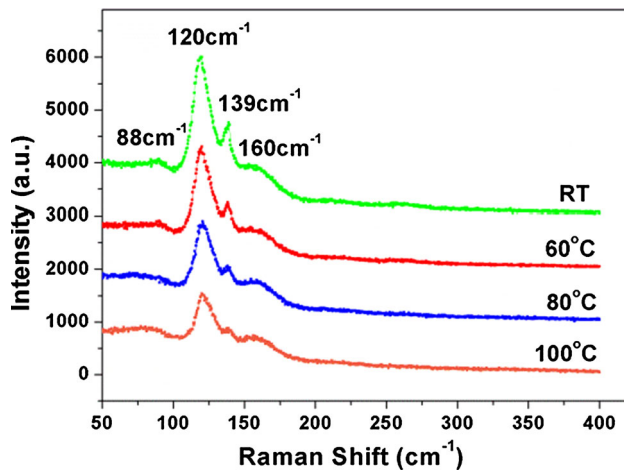
Fig. 5 Raman spectra for amorphous GeTe films prepared at various deposition temperatures

homopolar Te–Te bonds in the as-deposited state. It is known that homopolar Te–Te bonds are forbidden in the crystalline structure [10]. It has therefore been suggested that the presence of these homopolar Te–Te bonds might retard the crystallization process [9]. Our results suggest that the specific effect of Te–Te homopolar bonds is to raise the barrier for nucleation of the crystalline phase, rather than to impede crystal growth.

Effect of deposition rates

Figure 6 shows bright-field TEM images of GeTe films deposited at rates of 7.1 and 10.3 nm/min. The observed structures are similar to those of the films deposited at different temperatures (Fig. 1). The inset electron diffraction patterns confirm that the films are amorphous as deposited, which was also supported by XRD analysis. Using EDX, the composition of the films was determined to be $Ge_{47}Te_{53}$ (± 1 %), independent of the Ar pressure and sputtering rate.

Figure 7 shows XRD results for these films deposited at different sputtering rates. The as-deposited films were amorphous at all deposition rates, as shown in Fig. 7a. After annealing to 235 °C, the films were found to be fully crystallized, as shown in Fig. 7b. Regardless of the deposition rate, weak Te peaks were also observed due to the Te-rich composition of the films.

Figure 8a shows transformation curves for crystallization of GeTe, based on the maximum intensity of the (011) peak normalized by the magnitude of this peak after full transformation at 235 °C. . The samples were heated at a rate of 2 °C/min from room temperature to 235 °C. From the transformation curves, it is clearly seen that the apparent crystallization temperatures increase with increasing deposition rate. Figure 8b shows transformation
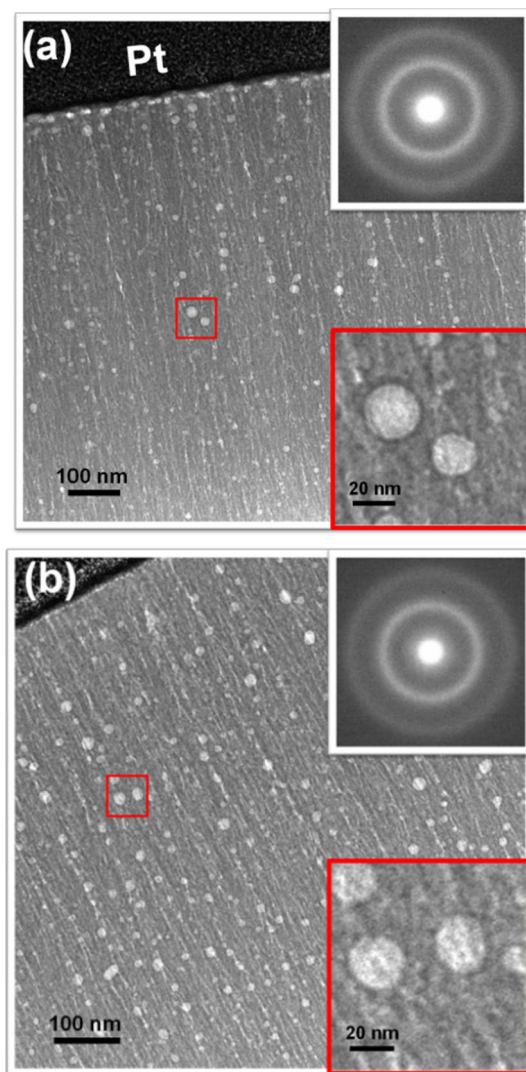

Fig. 6 Bright-field TEM images of cross sections of GeTe films deposited at deposition rates of **a** 7.1 nm/min and **b** 10.3 nm/min, on Si substrates coated with thin layers of native oxide. *Top right insets* show electron diffraction patterns and *bottom right insets* show high magnification views of nano-scale voids within the film. Pt layers on *top* of the films act as protective layers during FIB sample preparation

curves for GeTe films deposited at a rate of 7.1 nm/min and heated at different rates: 2, 5, and 10 °C/min.

The same approach discussed earlier was used to obtain the local effective activation energy E_α as a function of the fraction transformed α as shown in Fig. 9a. Figure 9b shows values of the activation energies for nucleation and growth obtained from the data in Fig. 9a. It is seen that the activation energy for nucleation increases with increasing deposition rate, from 3.5 to 4.0 eV. In contrast, the activation energy for growth remains constant at a value of 1.9 eV. Thus, the increase in the effective activation energy for crystallization of GeTe observed for increasing deposition rates is primarily
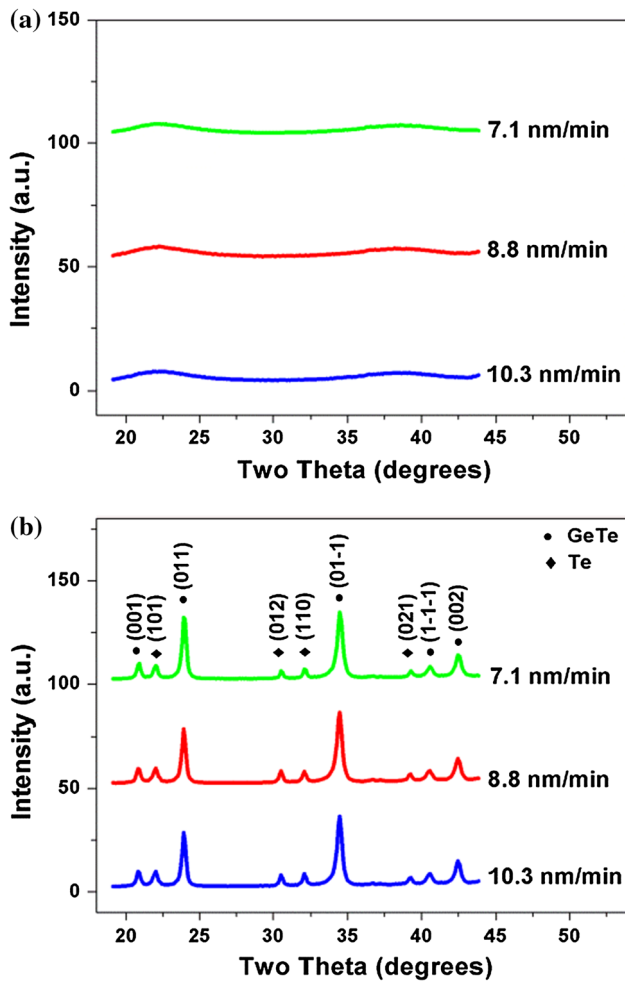
Fig. 7 XRD results for GeTe films. **a** as-deposited and **b** fully crystallized at 235 °C, for films deposited at different rates
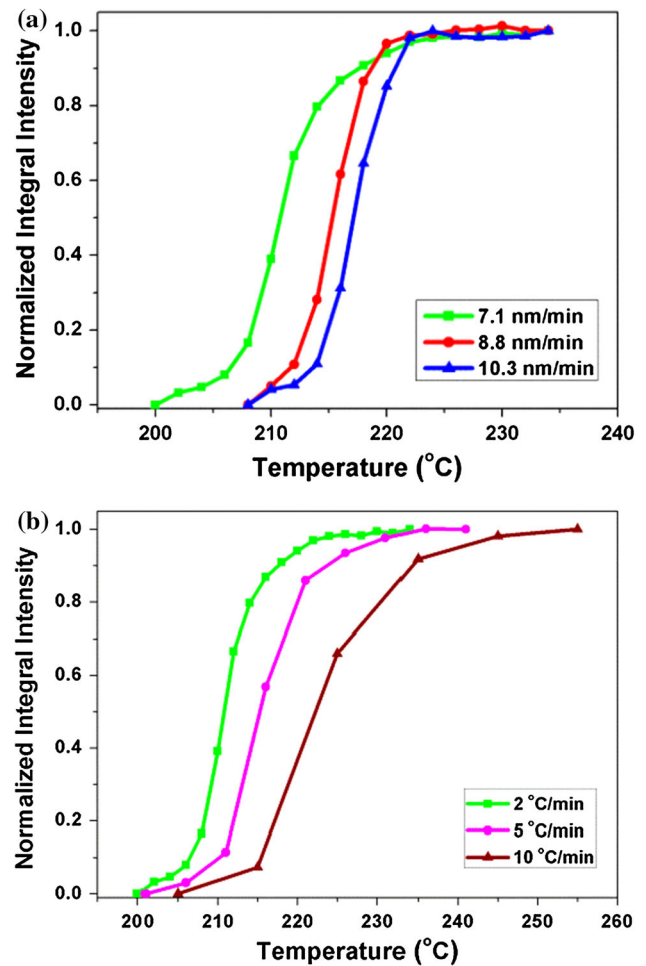

Fig. 8 **a** Transformation curves for GeTe films deposited at different deposition rates, normalized by the magnitude of the (011) peak observed at 235 °C, with a heating rate of 2 °C/min and **b** transformation curves for GeTe films deposited at a rate of 7.1 nm/min and heated at different rates

due to an increase in the activation energy for nucleation. It is expected that films deposited at higher deposition rates experience a higher effective quench rate [31]. This dependence on the effective quench rate is consistent with the results obtained for films deposited as different temperatures.

Figure 10 shows Raman spectra for GeTe films deposited at different rates. Similar to what was found for films deposited at different temperatures, two distinct peaks were also observed at 120 and 139 cm^{-1}, and their intensities increased with increasing deposition rate. This suggests the presence of homopolar Te–Te bonds in all the as-deposited films, regardless of the sputtering rate. However, this also shows that the number of Te–Te homopolar bonds increases with increasing deposition rate, which, we suggest, raises the barrier for nucleation of the crystalline phase.

Different sputtering targets were used in both sets of experiments. It should be noted that the film deposited at

room temperature in the first set of experiments exhibits higher activation energies for nucleation compared to those in the second set of experiments. This is likely due to the higher amount of excess Te in the first set of films, resulting from the use of different sputtering targets for the two sets of films. Work done by Carria et al. has shown that increasing amounts of excess Te will lead to a higher activation energy for crystallization [21]. However, this does not affect our interpretation of the data within a single set of samples having a fixed amount of access Te, and the correspondence of the trends observed for both sets. It has been shown through experiments carried out by others that Te–Te homopolar bonds exist even in stoichiometric amorphous GeTe films [37, 38]. We have also carried out experiments on stoichiometric Ge$_2$Sb$_2$Te$_5$ films deposited at varying substrate temperatures, with the XRD results and Raman spectra shown in Figs. S1 and S2 (Online
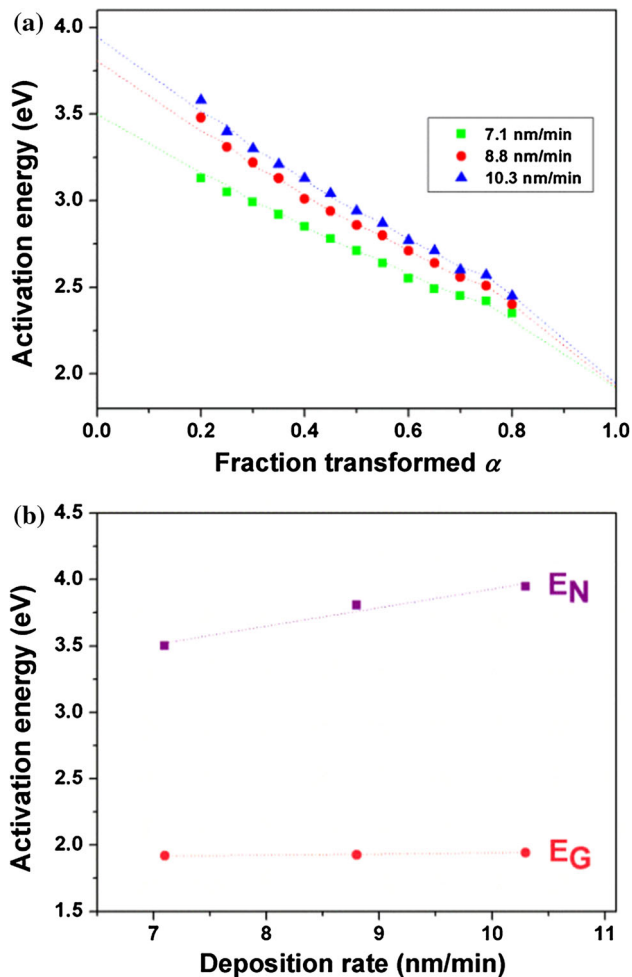
Fig. 9 **a** The local effective activation energy E_c as a function of the fraction transformed α for films prepared at various deposition rates and **b** activation energies for nucleation and growth as a function of the deposition rate

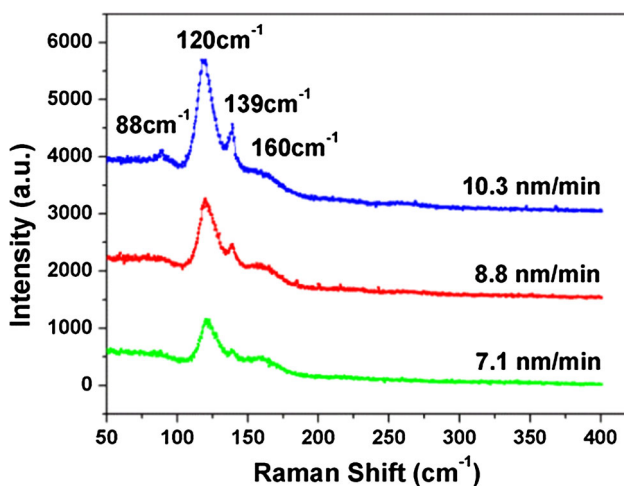**Fig. 10** Raman spectra for amorphous GeTe films prepared at various deposition rates

Resource 1). Even with stoichiometric $Ge_2Sb_2Te_5$ samples, the intensity of the 120 cm^{-1} Raman peak changes with the substrate temperature in a way that is analogous to what is seen for GeTe, and there are corresponding analogous changes in the crystallization behavior. This is consistent with other reported observations on stoichiometric GeTe and $Ge_2Sb_2Te_5$ films in which the crystallization rate is observed to decrease with the increased presence of homopolar Te–Te bonds [9, 10]. Taken together, these results support our proposition that the Te–Te bond density is the critical factor that affects crystal nucleation in the as-deposited films.

Summary and conclusions

We have studied the crystallization of amorphous GeTe films prepared by sputter deposition onto substrates held at different temperatures and deposited at different sputtering rates. Through analysis of the crystallization process carried out at different heating rates, it is shown that the deposition temperature and deposition rate have a significant effect on the nucleation of the crystalline phase, but a negligible effect on its growth. The activation energy for crystal nucleation increased with decreasing deposition temperature and with increasing deposition rate. Decreasing the deposition temperature and increasing the deposition rate both increase the effective quench rate. This highlights the influence of the effective quench rate on the crystallization of phase change materials. Raman spectral analysis indicates an increase of the number of homopolar Te–Te bonds with decreasing deposition temperature or increasing deposition rate. Given that homopolar bonds do not exist in the crystalline phase, we suggest that it is clustering of Te atoms in the films deposited at low temperatures and high rates that raises the barrier to nucleation of the crystalline phase.

References

1. Ovshinsky SR (1968) Reversible electrical switching phenomena in disordered structures. Phys Rev Lett 21(20):1450–1453

2. Kolobov AV, Fons P, Tominaga J (2007) Phase-change optical recording: past, present, future. Thin Solid Films 515(19):7534–7537

3. Wetnic W, Wuttig M (2008) Reversible switching in phase-change materials. Mater Today 11(6):20–27. doi:10.1016/S1369-7021(08)70118-4

4. Kolobov AV, Fons P, Frenkel AI, Ankudinov AL, Tominaga J, Uruga T (2004) Understanding the phase-change mechanism of rewritable optical media. Nat Mater 3:703–708

5. Wuttig M, Yamada N (2007) Phase-change materials for rewriteable data storage. Nat Mater 6:824–832

6. Lencer D, Salinga M, Grabowski B, Hickel T, Neugebauer J, Wuttig M (2008) A map for phase-change materials. Nat Mater 7:972–977

7. Raoux S, Wenic W, Lelmini D (2010) Phase change materials and their application to nonvolatile memories. Chem Rev 110(1):240–267. doi:10.1021/cr900040x

8. Lencer D, Salinga M, Wuttig M (2011) Design rules for phase-change materials in data storage applications. Adv Mater 23(18):2030–2058. doi:10.1002/adma.201004255

9. Carria E, Mio AM, Gibilisco S, Miritello M, d'Acapito F, Grimaldi MG, Rimini E (2011) Polymorphism of amorphous $Ge_2Sb_2Te_5$ probed by EXAFS and Raman spectroscopy. Electrochem Solid-State Lett 14(12):480–482. doi:10.1149/2.019112esl

10. Mio AM, Carria E, D'Arrigo G, Gibilisco S, Miritello M, Grimaldi MG, Rimini E (2011) Nucleation and grain growth in as deposited and ion implanted GeTe thin films. J Non-Cryst Solids 357(10):2197–2201. doi:10.1016/j.jnoncrysol.2011.02.042

11. Kissinger HE (1957) Reaction kinetics in differential thermal analysis. Anal Chem 29(11):1702–1706

12. Tamura N, MacDowell AA, Spolenak R, Valek BC, Bravman JC, Brown WL, Celestre RS, Padmore HA, Batterman BW, Patel JR (2003) Scanning X-ray microdiffraction with submicrometer white beam for strain/stress and orientation mapping in thin films. J Synchrotron Radiat 10:137–143. doi:10.1107/S0909049502021362

13. Kunz M, Tamura N, Chen K, MacDowell AA, Celestre RS, Church MM, Fakra S, Domning EE, Glossinger JM, Kirschman JL, Morrison GY, Plate DW, Smith BV, Warwick T, Yashchuk VV, Padmore HA, Ustundag E (2009) A dedicated superbend X-ray microdiffraction beamline for materials, geo-, and environmental sciences at the advanced light source. Rev Sci Instrum 80(3):035108. doi:10.1063/1.3096295

14. Andrikopoulos KS, Yannopoulos SN, Voyiatzis GA, Kolobov AV, Ribes M, Tominaga J (2006) Raman scattering study of the a-GeTe structure and possible mechanism for the amorphous to crystal transition. J Phys 18(3):965–979. doi:10.1088/0953-8984/18/3/014

15. Bales GS, Zangwill A (1991) Macroscopic model for columnar growth of amorphous films by sputter deposition. J Vac Sci Technol A 9(1):145–149. doi:10.1116/1.577116

16. Tsukimoto S, Moriyama M, Murakami M (2004) Microstructure of amorphous tantalum nitride thin films. Thin Solid Films 460(1–2):222–226. doi:10.1016/j.tsf.2004.01.073

17. Tamura N (2014) XMAS: a versatile tool for analyzing synchrotron X-ray microdiffraction data, in strain and dislocation gradients from diffraction: spatially-resolved local structure and defects. Imperial College Press, London

18. Matsunaga T, Kojima R, Yamada N, Kifune K, Kubota Y, Tabata Y, Takata M (2006) Single structure widely distributed in a $GeTe - Sb_2Te_3$ pseudobinary system: a rock salt structure is retained by intrinsically containing an enormous number of vacancies within its crystal. Inorg Chem 45(5):2235–2241. doi:10.1021/ic051677w

19. Ghezzi GE, Morel R, Brenac A, Boudet N, Audier M, Fillot F, Maitrejean S, Hippert F (2012) Crystallization of $Ge_2Sb_2Te_5$ nanometric phase change material clusters made by gas-phase condensation. Appl Phys Lett 101(23):233113–233114

20. Gourvest E, Lhostis S, Kreisel J, Armand M, Maitrejean S, Roule A, Vallee C (2009) Evidence of germanium precipitation in phase-change $Ge_{1-x}Te_x$ thin films by Raman scattering. Appl Phys Lett 95(3):031908. doi:10.1063/1.3186077

21. Carria E, Mio AM, Gibilisco S, Miritello M, Bongiorno C, Grimaldi MG, Rimini E (2012) Amorphous-crystal phase transitions in Ge_xTe_{1-x} alloys. J Electrochem Soc 159(2):H130–H139. doi:10.1149/2.048202jes

22. Friedrich I, Weidenhof V, Njoroge W, Franz P, Wuttig M (2000) Structural transformations of $Ge_2Sb_2Te_5$ films studied by electrical resistance measurements. J Appl Phys 87(9):4130–4134

23. Choi Y, Jung M, Lee Y-K (2009) Effect of heating rate on the activation energy for crystallization of amorphous $Ge_2Sb_2Te_5$ thin film. Electrochem Solid-State Lett 12(7):F17–F19. doi:10.1149/1.3129137

24. Abu El-Oyoun M (2009) Determination of the crystallization kinetic parameters of $Ge_{22.5}Te_{77.5}$ glass using model-free and model-fitting methods. J Alloys Compd 486(1–2):1–8. doi:10.1016/j.jallcom.2009.06.137

25. Kasyap S, Patel A, Pratap A (2014) Crystallization kinetics of $Ti_{20}Zr_{20}Cu_{60}$ metallic glass by isoconversional methods using modulated differential scanning calorimetry. J Therm Anal Calorim 116(3):1325–1336. doi:10.1007/s10973-014-3753-z

26. Dohare C, Mehta N (2012) Iso-conversional kinetic study of non-isothermal crystallization in glassy $Se_{98}Ag_2$ alloy. J Therm Anal Calorim 109(1):247–253. doi:10.1007/s10973-011-1696-1

27. Wei L, Biao Y, Wen-hai H (2005) Complex primary crystallization kinetics of amorphous Finemet alloy. J Non-Cryst Solids 351(40–42):3320–3324. doi:10.1016/j.jnoncrysol.2005.08.018

28. Majhi K, Varma KBR (2009) Crystallization kinetic studies of $CaBi_2B_2O_7$ glasses by non-isothermal methods. J Mater Sci 44:385–391. doi:10.1007/s10853-008-3149-1

29. Soares RS, Monteiro RCC, Lima MMRA, Sava BA, Elisa M (2014) Phase transformation and microstructural evolution after heat treatment of a terbium-doped lithium-aluminum phosphate glass. J Mater Sci 49:4601–4611. doi:10.1007/s10853-014-8162-y

30. Lu QM, Libera M (1995) Microstructural measurements of amorphous GeTe crystallization by hot-stage optical microscopy. J Appl Phys 77(2):517–521. doi:10.1063/1.359034

31. Chu JP, Lai YW, Lin TN, Wang SF (2000) Deposition and characterization of TiNi-base thin films by sputtering. Mater Sci Eng A A277(1–2):11–17. doi:10.1016/S0921-5093(99)00560-2

32. Jeyasingh R, Fong SW, Lee J, Li Z, Chang K-W, Mantegazza D, Asheghi M, Goodson KE, Wong HSP (2014) Ultrafast characterization of phase-change material crystallization properties in the melt-quenched amorphous phase. Nano Lett 14(6):3419–3426. doi:10.1021/nl500940z

33. Orava J, Hewak DW, Greer AL (2015) Fragile-to-strong crossover in supercooled liquid Ag-In-Sb-Te studied by ultrafast calorimetry. Adv Funct Mater 25(30):4851–4858. doi:10.1002/adfm.201501607

34. Andrikopoulos KS, Yannopoulos SN, Kolobov AV, Fons P, Tominaga J (2007) Raman scattering study of GeTe and $Ge_2Sb_2Te_5$ phase-change materials. J Phys Chem Solids 68(5–6):1074–1078. doi:10.1016/j.jpcs.2007.02.027

35. Mazzarello R, Caravati S, Angioletti-Uberti S, Bernasconi M, Parrinello M (2010) Signature of tetrahedral Ge in the Raman

spectrum of amorphous phase-change materials. Phys Rev Lett 104(8):085503

36. Pine AS, Dresselhaus G (1971) Raman spectra and lattice dynamics of tellurium. Phys Rev B 4(2):356–371

37. Fisher G, Tauc J, Verhelle Y (1974) Amorphous and liquid semiconductors. Taylor and Francis, London

38. Hosokawa S, Hari Y, Kouchi T, Ono I, Sato H, Taniguchi M, Hiraya A, Takata Y, Kosugi N, Watanabe M (1998) Electronic structures and local atomic configurations in amorphous GeSe and GeTe. J Phys 10(8):1931–1950. doi:10.1088/0953-8984/10/8/024